Spin Valve-Based Rhombus-Shaped Microobject Implementing Full Wheatstone Bridge

Mikhail Milyaev *, Larisa Naumova, Anastasiya Germizina, Tatyana Chernyshova, Anastasia Pavlova, Tatiana Krinitsina, Vyacheslav Proglyado, Vladimir Ustinov

Posted Date: 5 December 2023

doi: 10.20944/preprints202312.0210.v1

Keywords: spin valve; Wheatstone bridge; magnetic anisotropy; shape anisotropy; exchange bias field

Article

Spin Valve-Based Rhombus-Shaped Microobject Implementing Full Wheatstone Bridge

Mikhail Milyaev *, Larisa Naumova, Anastasia Germizina, Tatyana Chernyshova, Anastasia Pavlova, Tatiana Krinitsina, Vyacheslav Proglyado and Vladimir Ustinov

M.N. Mikheev Institute of Metal Physics, Ural Branch, Russian Academy of Sciences, S. Kovalevskoi Street 18, Ekaterinburg, 620990, Russia

* Correspondence: milyaev@imp.uran.ru; Tel.: +7 (343) 374-38-81

Abstract: Spin valves with a synthetic antiferromagnet were fabricated by magnetron sputtering. It was shown that the fabricated spin valves had perfect microstructure of layers and smooth interfaces, therefore RKKY interaction dominates in coupling of ferromagnetic layers separated by a copper spacer. Rhombus-shaped microobjects were fabricated from a single spin valve film. The thermomagnetic treatment procedure was found, to form unidirectional anisotropy in the microobject so, that the values of the exchange bias fields in the rhombus' nonparallel sides were opposite in sign. For the synthetic antiferromagnet CoFeNi/Ru/CoFeNi the difference between ferromagnetic layers thicknesses was found, at which the thermomagnetic treatment forms the same exchange bias all over the rhombus' side. The sensor element was fabricated in which each side of the rhombus was a shoulder of a Wheatstone bridge. After the thermomagnetic treatment procedure each shoulder worked as an active magnetosensitive element, thus the device operated as the full Wheatstone bridge. The sensor output has the shape of a step, high sensitivity to field change and significant magnetic hysteresis. Such characteristics are suitable for switching devices.

Keywords: spin valve; Wheatstone bridge; magnetic anisotropy, shape anisotropy, exchange bias field

1. Introduction

Bridge circuit measurements have important advantages such as low measurement error, high sensitivity, reduction of noise and temperature drift [1]. Wheatstone bridge electrical circuit consists of two parallel branches each consisting of two arms with resistor element in it. If a Wheatstone bridge is used in magnetic field sensors, then the elements electrical resistivity of which depends on the applied magnetic field are used as the resistors in each arm. The supply voltage U_{in} is applied to the parallel branches and the potential difference U_{out} between middle points of the branches is measured. The maximum of U_{out}/U_{in} can be achieved if resistance increases in two bridge arms and decreases in two other arms with the change of magnetic field. In this case, all four sensitive elements contribute to the output signal, and circuit is the full-bridge. In microelectronics, a spin valve (SV) nanostructure with the giant magnetoresistance (GMR) is often used as magnetosensitive material [2–4].

SV consists of two ferromagnetic (FM) layers, so-called free (FL) and pinned (PL), separated by a non-magnetic spacer usually from Cu. The magnetic moment ($\mathbf{M}_p$) of the pinned layer is fixed by the exchange interaction with the adjacent antiferromagnetic (AF) layer [5]. The magnetic reversal hysteresis loop for PL is shifted to the high-field region. The high-field loop shift (H_{ex}) depends on the interaction between AF and PL. For FL the field shift of the hysteresis loop from $H = 0$ (H_j) is small. In the fields $|H_j| < |H| < |H_{ex}|$ the magnetic moments of FL and PL are opposite and there is a plateau on the magnetoresistive curve corresponding to the maximum of magnetoresistance (MR_{max}). H_j depends on FM layers interaction through the non-magnetic spacer. This interaction is the result of competition between dipolar ferromagnetic and oscillating RKKY exchange interactions [6]. If dipolar ferromagnetic interaction is dominant, then H_j and MR_{max} decrease with the increase of spacer

 doi:10.20944/preprints202312.0210.v1

thickness. If the standard deviation of interlayer roughness is no more than 0.3–0.5 nm [7,8], then RKKY interaction can be dominant. In this case, H_j changes periodically with the increase of spacer thickness, and SV with $H_j \approx 0$ and large MR_{max} can be obtained [9].

The pinned layer in SV can be replaced by the synthetic antiferromagnet (SAF) to reduce the magnetostatic interaction between the FM layers and to increase the operating temperature range. SAF consists of two FM layers coupled through the layer of Ru [10]. Thickness of Ru layer (0.7-0.9 nm) corresponds to the maximum of antiferromagnetic exchange interaction [11]. In this case the FM layer adjacent to the AF layer is called the pinned layer (PL) and the second FM layer in SAF is called the reference layer (RL).

Magnetic and magnetoresistive properties of SV have several types of anisotropy: 1) uniaxial easy-axis (EA) anisotropy induced during deposition in a magnetic field; 2) unidirectional anisotropy with the pinning direction (PD) arising due to the interaction between the pinned and AF layers; and 3) shape anisotropy in micro-objects. PD can be changed by the thermomagnetic treatment (TMT) [1,12].

It is quite difficult to implement a full Wheatstone bridge at magnetic field microsensors fabrication from a single SV film, because the resistance (R_n, n = 1, 2, 3, 4) of all bridge arms changes equally at the change of a magnetic field, and all dR_n/dH are the same in sign. $dR_{1,3}/dH$ and $dR_{2,4}/dH$ should be opposite in sign to give a contribution to the output voltage U_{out} from all bridge elements. It is possible for SVs in a Wheatstone bridge if their PD are mutually opposite. The following methods are used to obtain this: two stage deposition of SVs with different PD [1] and EA [13] or with different compositions [14] onto the corresponding parts of the substrate; TMT in a field corresponding to the spin-flop state in the SAF [11,13]; the use of a permanent magnet to create additional oppositely directed field components in the active elements of the bridge [15].

In this work the spin valves with a predominance of RKKY interaction between the free and reference layers are studying. The formation of an exchange shift in the pinned layer under combination of shape anisotropy and uniaxial anisotropy is investigated. A thermomagnetic treatment mode to form an opposite exchange shift in the non-parallel sides of a rhombus-shaped microobject was found and full Wheatstone bridge circuit was realized.

2. Materials and Methods

SVs with the composition $Ta(5)/[Ni_{80}Fe_{20}]_{60}Cr_{40}(5)/Co_{70}Fe_{20}Ni_{10}(t_{FL})/Cu(t_{Cu})/Co_{70}Fe_{20}Ni_{10}(t_{RL})/Ru(0.8)/Co_{70}Fe_{20}Ni_{10}(t_{PL})/Fe_{50}Mn_{50}(18)/Ta(6)$ were deposited on glass substrates by dc magnetron sputtering in the magnetic field of 80 Oe applied in a film plane. Layer thicknesses are given in nm. The thicknesses of Cu and FM layers were varied. $Co_{70}Fe_{20}Ni_{10}$ was used as FM layer. For this alloy the saturation magnetization is 13% higher and the coercivity is 4.5 times lower than for $Co_{90}Fe_{10}$ commonly used in SVs [16]. The buffer layer $Ta/[Ni_{80}Fe_{20}]_{60}Cr_{40}$ promotes the formation of <111> texture [17,18] and the decrease of crystallites size and interlayer roughness of nanostructured film [19].

Studies of materials microstructure were carried out by X-ray diffractometry on a DRON-3M difactometer in $CoK\alpha_1$ radiation and by transmission electron microscopy on a Tecnai G-30.

Magnetic microstructure of microobjects was investigated by scanning probe microscope Solver Next (NT-MDT) in the magnetic force microscopy (MFM) mode.

Magnetoresistive measurements and TMT were carried out in a setup based on a Bruker electromagnet and a LakeShore 336 temperature controller. TMT involved heating in a helium atmosphere to a temperature T_{TMT} = 448 K, which exceeds the blocking temperature T_b = 433 K for SVs based on an antiferromagnetic FeMn alloy [20]. The magnetoresistance was determined as $MR = (R(H) - R_s)/R_s$, where $R(H)$ – resistance of the sample in a magnetic field, R_s – resistance of the sample in the saturation field.

Microobjects were fabricated by laser lithography on DWL 66+ (Heidelberg Instruments Mikrotechnik GmbH) and reactive ion etching on PlasmaPro 80 RIE (Oxford Instruments). The contact pads were fabricated using the lift-off procedure. There were prepared 2 types of microobjects (Figure 1). (1) V-shaped microobjects were made of two microstripes forming a corner with Cu

Preprints (www.preprints.org) | NOT PEER-REVIEWED | Posted: 5 December 2023 doi:10.20944/preprints202312.0210.v1

contact pads at the apex of the corner and at the ends of the microstripes. The corner angle (α) was 20 or 40º, and its bisector was coincided with the EA. (2) Rhombus-shaped microobjects were made of 315 μm long and 2 μm wide microstripes and Cu pads at the rhombus vertices. The acute angles were α = 20 or 40º, and the long rhombus diagonal was coincided with the EA.

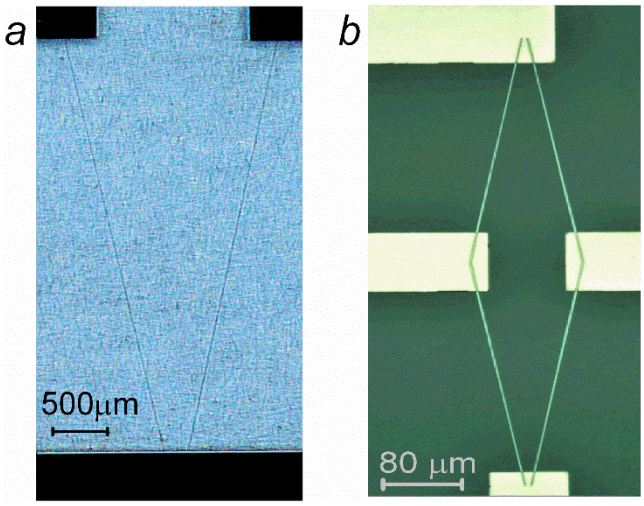

Figure 1. Images of V-shaped (**a**) and rhombus-shaped (**b**) microobject with contact pads.

3. Results

3.1. Microstructural studies

The $Co_{70}Fe_{20}Ni_{10}$, $[Ni_{80}Fe_{20}]_{60}Cr_{40}$ ternary FM alloys, Cu and $Fe_{50}Mn_{50}$ antiferromagnetic alloy have the same cubic face-centered (fcc) crystal structure and similar lattice parameter values. Figure 2 shows coincidence of the angular position of (111) peak for bulk $Co_{70}Fe_{20}Ni_{10}$ alloy, thin film of $Co_{70}Fe_{20}Ni_{10}$ alloy and for the SV containing the layers of these alloys. It is seen that there is <111> texture in the film and in the SV, since there are no other peaks of the fcc structure. The full width at half-maximum of the rocking curve (ω-scan) for (111) peak of SV is 4.4 degrees.

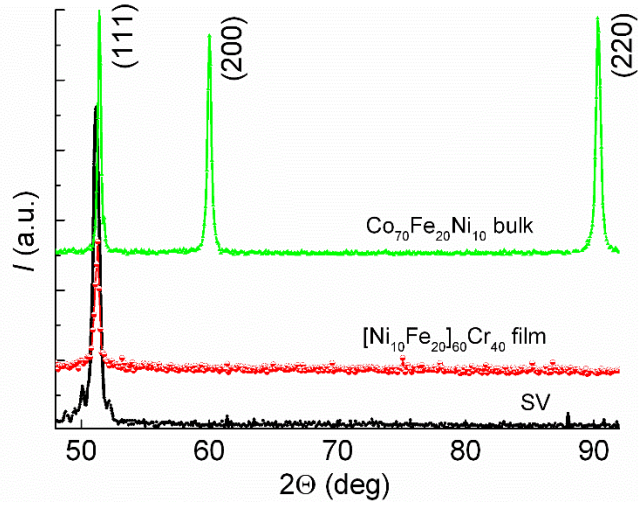

Figure 2. X-ray diffraction patterns for SV of Ta(5)/NiFeCr(5)/CoFeNi(3.5)/Cu(3.3)/CoFeNi(3.5) /Ru(0.8)/CoFeNi(3)/FeMn(10)/Ta(5) composition, NiFeCr film with thickness of 60 nm and bulk sample of CoFeNi alloy.

Thickness oscillations (satellites) are clearly seen around (111) peak in SV X-ray diffraction pattern. The thickness estimated by the period of these oscillations coincides with the total thickness of the NiFeCr/CoFeNi/Cu/CoFeNi layers of the SV. Thus in that part of nanostructure alignment of the microstructure of the layers takes place.

Preprints (www.preprints.org) | NOT PEER-REVIEWED | Posted: 5 December 2023 doi:10.20944/preprints202312.0210.v1

Figure 3 shows the results of TEM investigation. In electron diffraction pattern Debye rings for NiFeCr, CoFeNi, Cu and FeMn are common because of the same fcc structure and similar lattice parameter. Note that {220} ring is the brightest, and {111} ring is weak. This is characteristic for <111> texture and consistent with the results of the X-ray diffraction study. High-resolution images show thin parallel bands (Figure 3a). It is direct resolution of atomic plane projections on the image plane. Figure 3 b shows moire lines. This is the result of the interference of diffracted by the crystal lattices of adjacent layers electron beams. In multilayer structures such parallel to each other moire lines appear if the lattice mismatch of layers is low and the number of dislocations and packaging defects is small.

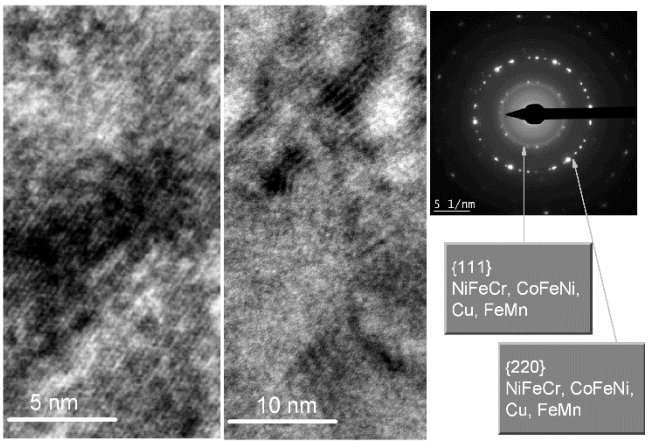

Figure 3. TEM high-resolution images and electron diffraction pattern for SV of Ta(5)/NiFeCr(5)/CoFeNi(3.5)/Cu(3.3)/CoFeNi(3.5)/Ru(0.8)/CoFeNi(3)/FeMn(10)/Ta(5) composition.

So, studied SVs have perfect microstructure of layers, low lattice mismatch of layers and high perfection of <111> texture. Such properties of microstructure were obtained by using layer materials with similar crystal structure and the buffer layer of the Ta(5)/NiFeCr(5) composition. In [9,19] the similar high-quality microstructure was achieved in superlattices and spin valves sputtered onto Ta/NiFeCr buffer layer. In present investigation, we need such microstructural properties to obtain smooth interfaces and RKKY interlayer coupling prevalence.

3.2. Exchange coupling of free and reference layers

Magnetoresistive curves were measured for SVs with various t_{Cu} = 1.8 – 2.4 nm in a field applied parallel to PD || EA. Figure 4 shows $MR(H)$ curve for SV with t_{Cu} = 2.2 nm. It is seen from the figure how the values of MR_{max} and the shift of low field hysteresis loop (H_j) were estimated.

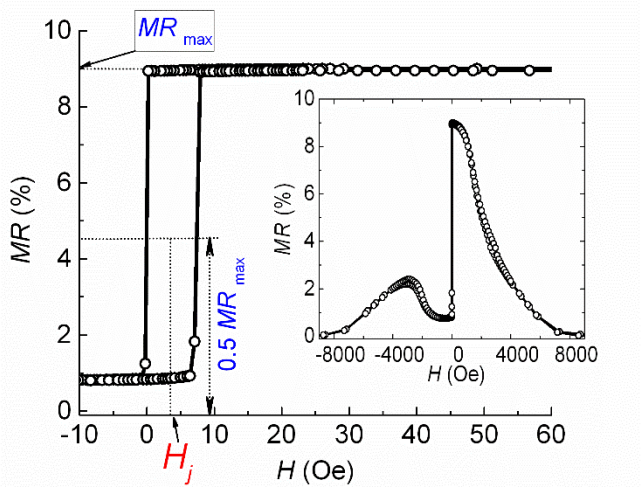

Figure 4. Low field part of magnetoresistive curve for SV of Ta(5)/NiFeCr(5)/CoFeNi(5.5)/Cu(2.2)/ CoFeNi(2.3)/Ru(0.8)/CoFeNi(2)/ FeMn(10)/Ta(5) composition. The inset shows the $MR(H)$ curve in a wide range of fields.

Preprints (www.preprints.org) | NOT PEER-REVIEWED | Posted: 5 December 2023 doi:10.20944/preprints202312.0210.v1

The H_j value depends on the interaction between free and reference FM layers. Ordinarily, if the ferromagnetic dipolar coupling dominates, then $H_j(t_{Cu})$ dependence decreases monotonously. In our case $H_j(t_{Cu})$ dependence has an oscillating character, and we may conclude that RKKY interlayer coupling dominates (Figure 5).

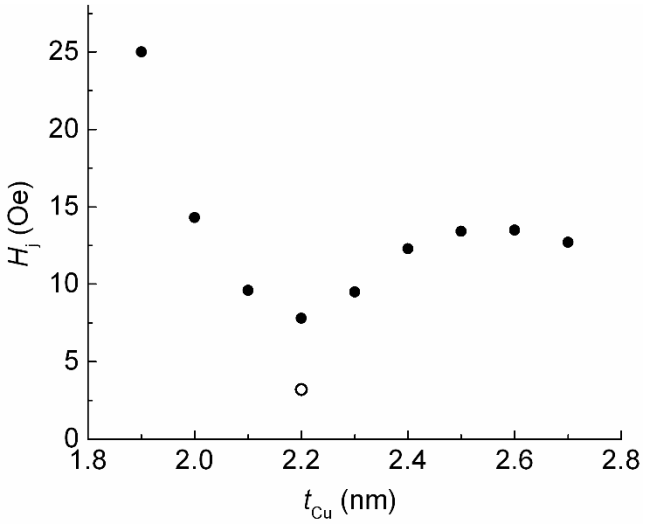

Figure 5. The dependence of low field hysteresis loop shift on the thickness of Cu layer for SVs of Ta(5)/NiFeCr(5)/CoFeNi(4)/Cu(t_{Cu})/CoFeNi(4)/Ru(0.8)/CoFeNi(3.5)/FeMn(10)/Ta(5) composition (solid symbols) and the shift of low field hysteresis loop for the SV of Ta(5)/NiFeCr(5)/CoFeNi(5.5)/Cu(2.2)/CoFeNi(2.3)/Ru(0.8)/CoFeNi(2)/ FeMn(10)/Ta(5) composition (open symbol).

Minimum value of H_j was obtained at t_{Cu} = 2.2 nm. Then we changed the thickness of FM layers in order to increase MR_{max} and further reduce the H_j. We achieved the H_j value close to H = 0 (open symbol in the Figure 5) and MR_{max} = 9 % . In the SV of obtained composition, we changed the reference layer thickness (t_{RL}). Thus, the difference (t_{RL} – t_{PL}) between FM layers in SAF and the total magnetic moment of SAF changed, respectively. Figures 6 and 7 show change of magnetoresistive curves and the values of H_j and MR_{max} that occur due to increasing value of t_{RL}.

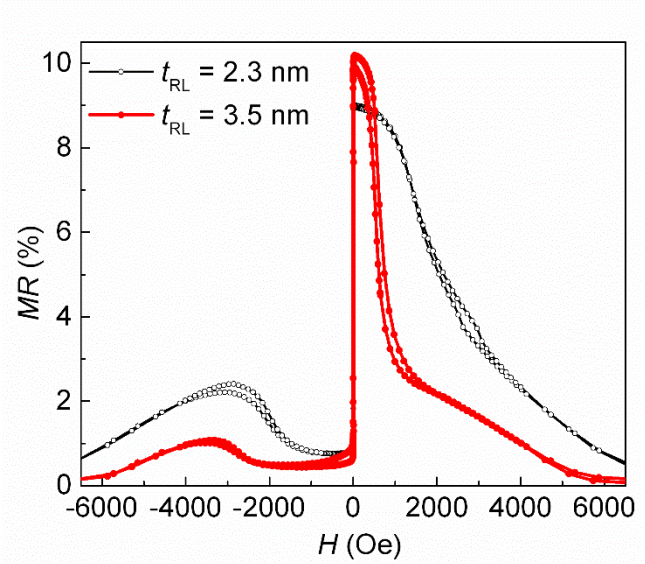

Figure 6. Magnetoresistive curves for SVs of Ta(5)/NiFeCr(5)/CoFeNi(5.5)/Cu(2.2)/ CoFeNi(t_{RL})/Ru(0.8)/CoFeNi(2)/ FeMn(10)/Ta(5) composition for t_{RL} = 2.3 and 3.5 nm.

Preprints (www.preprints.org) | NOT PEER-REVIEWED | Posted: 5 December 2023 doi:10.20944/preprints202312.0210.v1

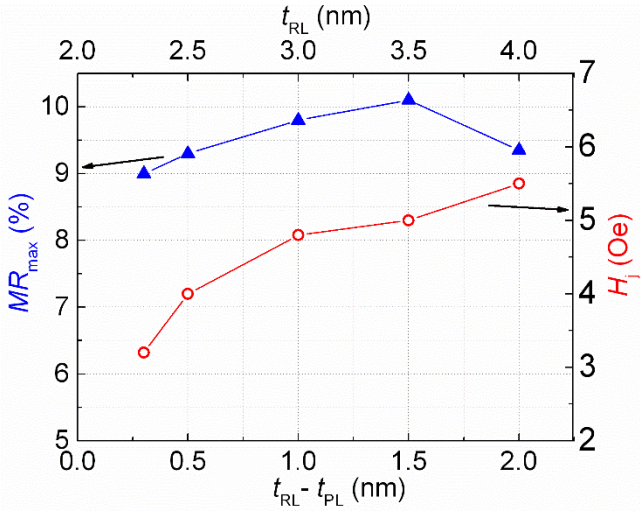

Figure 7. Dependencies of low field hysteresis loop shift and the maximal magnetoresistance on the reference layer thickness for the SVs of Ta(5)/NiFeCr(5)/CoFeNi(5.5)/Cu(2.2)/ CoFeNi(t_{RL})/Ru(0.8)/CoFeNi(2)/ FeMn(10)/Ta(5) composition.

It can be seen that when the thickness and, accordingly, the magnetic moment of the reference layer increases, the interlayer coupling and the H_j value naturally increase. Note that the value of MR_{max} varies slightly.

Further studies will be carried out on this series of SVs with a small shift of the low-field hysteresis loop and different values of the reference layer magnetic moment.

3.3. Change of pinning direction in spin valve films and microobjects during thermomagnetic treatment

Thermomagnetic treatment procedure includes annealing at T_{TMT} and subsequent cooling in the applied magnetic field H_{TMT}. If $T_{TMT} > T_b$, the exchange interaction at the boundary CoFeNi/FeMn is destroyed, then the initial unidirectional anisotropy and the initial PD in the SV disappear. Cooling in the applied magnetic field forms new unidirectional anisotropy and new PD1. The direction of PD1 coincides with direction of magnetic moment of adjacent FM layer [21,22]. We performed two consecutive TMT procedures for the following objects: V-shaped SV microobject and SV film. We performed the first TMT(1) in H_{TMT} = 9 kOe exceeding the magnetic saturation field and the second TMT(2) in $H_{TMT} \approx 0$. H_{TMT} was always directed perpendicular to EA. After TMT(2) we investigated the magnetic structure of V-shaped microobject and SV film using magnetic force microscopy. Figure 8 shows topography and corresponding MFM images obtained for the film and for V-shaped microobject.

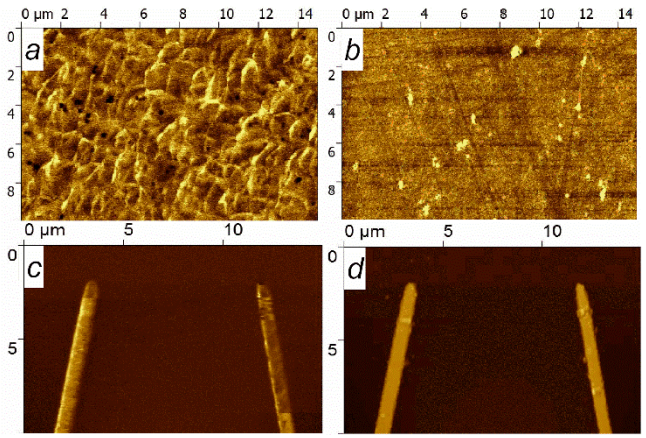

Figure 8. Topography (**b**,**d**) and MFM (**a**,**c**) images obtained for the film (**a**,**b**) and for V-shaped microobject (**c**,**d**).

Preprints (www.preprints.org) | NOT PEER-REVIEWED | Posted: 5 December 2023 doi:10.20944/preprints202312.0210.v1

The MFM image of the film shows an irregular magnetic structure. Each of the two stripes of the V-shaped microobject is in an almost single-domain state. Magnetic contrast shows that the magnetic ordering in these stripes is different. In MFM image (Figure 8c) left stripe is lighter than right stripe while there is no such difference in the topography image. Thus, after the same TMT, different magnetic structures are formed in the film and in V-shaped microobject. Presumably, the reason of the observed differences is as follows.

Magnetic moments of pinned and reference layer ($\mathbf{M}_{PL}$ and $\mathbf{M}_{RL}$) are antiferromagnetically coupled and opposite to each other in $H_{TMT} \approx 0$. In the SV film during TMT(2) at $T = T_{TMT}$ uniaxial anisotropy controls the turn of $\mathbf{M}_{PL}$ and $\mathbf{M}_{RL}$, thus the clockwise and counterclockwise turns are equally probable (Figure 9). During subsequent cooling, the exchange interaction in CoFeNi/FeMn boundary fixes this different magnetic ordering and forms new pinning directions PD1 and PD2 in different regions of the film. PD1 and PD2 are antiparallel and collinear with EA. In microobjects, shape anisotropy competes with uniaxial anisotropy. If shape anisotropy dominates, then it controls the turn of $\mathbf{M}_{PL}$ and $\mathbf{M}_{RL}$ during TMT(2) at $T = T_{TMT}$. With our experiment geometry (Figure 9) in one stripe of V-shaped microobject $\mathbf{M}_{PL}$ and $\mathbf{M}_{RL}$ will turn clockwise, and in the other – counterclockwise. Thus after the cooling new pinning directions PD1and PD2 are collinear with stripes. If the angle between the stripes is 20 or 40°, the angle between PD1 and PD2 will be 160 or 140°, respectively.

Magnetoresistive curves measured for each stripe of V-shaped microobject in the magnetic field applied parallel to EA are shown in Figure 10. The values of H_{ex} for two different stripes are opposite in sign. This is in a good agreement with the fact that in one stripe the projection of PD onto the applied field is positive, and in the other - negative.

In the low fields $dMR/dH > 0$ for the green magnetoresistive curve and $dMR/dH < 0$ for the blue magnetoresistive curve. Note that this PD arrangement was obtained in different stripes of a single microobject by two TMT in a direction-fixed magnetic field.

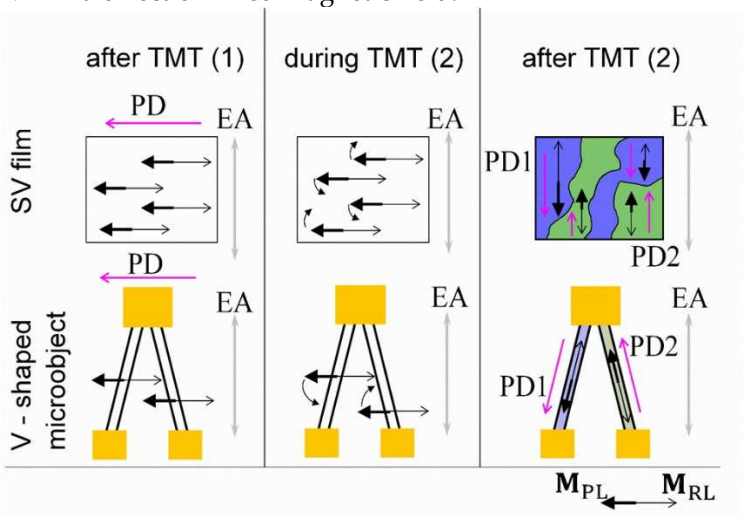

Figure 9. Schematic representation of turn of reference and pinned layer magnetic moments in SV film and SV microobject during TMT.

Preprints (www.preprints.org) | NOT PEER-REVIEWED | Posted: 5 December 2023 doi:10.20944/preprints202312.0210.v1

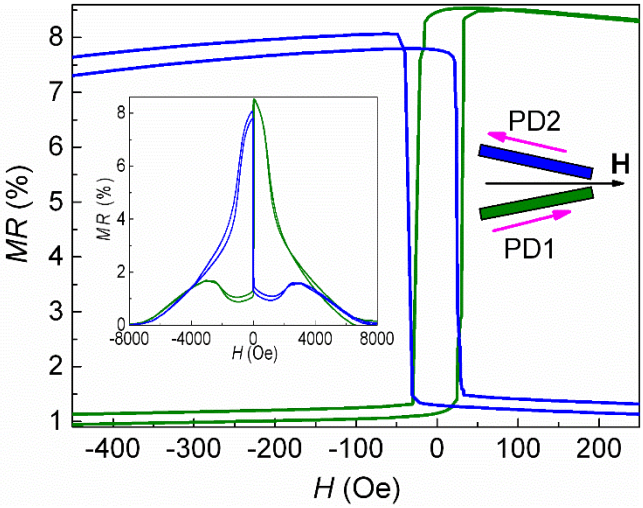

Figure 10. Low field parts of magnetoresistive curves measured for each stripe of V-shaped SV microobject. The applied magnetic field direction with respect to PD1 and PD2 is shown in the insert on the right. The inset on the left shows the *MR*(*H*) curves in a wide range of fields. .

3.4. Full Wheatstone Bridge based on rhombus-shaped spin valve microobject

TMT(1) and TMT(2) procedures were performed for rhombus-shaped spin valve microobject. Figure 11 shows the PD arrangement in rhombus sides which can be expected if you consider a rhombus as two V-shaped microobjects. It is this mutual PD arrangement that is required to implement the Wheatstone bridge, in which $dR_{1,3}/dH$ and $dR_{2,4}/dH$ are opposite in sign, thus each SV-element makes an active contribution to the output signal.

We applied supply voltage (U_{in}) to the long diagonal and measured output voltage (U_{out}) in the short diagonal of the rhombus under a magnetic field swept along EA (Figure 12).

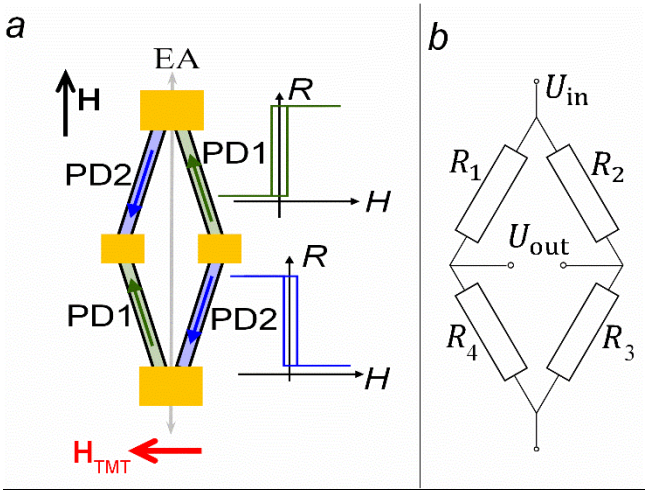

Figure 11. Scheme of PD arrangement in rhombus-shaped microobject sides after TMT(1) and TMT(2) (a) and electric circuit of the Wheatstone bridge (b). The inset in (a) shows *R*(*H*) dependences for R_1, R_3 (blue) and R_2, R_4 (green).

Preprints (www.preprints.org) | NOT PEER-REVIEWED | Posted: 5 December 2023 doi:10.20944/preprints202312.0210.v1

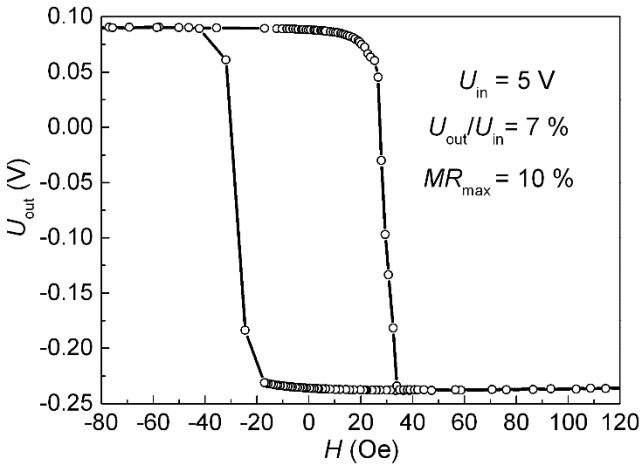

Figure 12. Wheatstone bridge output under a magnetic field sweep along EA for the rhombus-shaped microobject based on SV of Ta(5)/NiFeCr(5)/CoFeNi(5.5)/Cu(2.2)/CoFeNi(3.5)/ Ru(0.8)/CoFeNi(2)/ FeMn(10)/Ta(5) composition.

Maximal output of full Wheatstone bridge is estimated from $U_{out}/U_{in} = \Delta R/R$, where R is the resistance of each of the four elements and ΔR is a resistance change in the applied magnetic field. For half Wheatstone bridge with two active sensing elements, maximal output is $U_{out}/U_{in} = 0.5\Delta R/R$, accordingly [23]. Thus, for full Wheatstone bridge with for active SV-elements we obtain $U_{out}/U_{in} = MR_{max}$, where MR_{max} is maximal magnetoresistance of each SV-element. In our case U_{out}/U_{in} = 7 % while MR_{max} = 10 % (Figures 6 and 12), thus $0.5MR_{max} < U_{out}/U_{in} < MR_{max}$. A possible reason is that there are small areas of undesirable PD orientation in the rhombus -forming stripes. These areas are visible in the image of the magnetic structure (Figure 8c) in the upper part of the left stripe and in the lower part of the right stripe.

3.5. Formation of opposite pinning directions in rhombus-shaped microobjects based on spin valves with different thickness of the reference layer

An increase in the thickness t_{RL} leads to an increase of the total effective magnetic moment ($\mathbf{M}_{eff}$) of antiferromagnetically coupled $\mathbf{M}_{PL}$ and $\mathbf{M}_{RL}$, $M_{eff} = M_{RL} - M_{PL}$. During TMT(2) at $T > T_b$ the magnetic moments arrange in accordance to minimize the anisotropy energy. We estimate the shape anisotropy field, using [24] where the demagnetizing factors of the general ellipsoid were reported. For the long stripe, the demagnetizing factor is approximately t/w, where t is the thickness of the FM layer and w is the width of the stripe. Hence, the anisotropy field is the sum of two terms: $H_a = 2K_u/M_{eff} + 4\ M_{eff}\ t/w$, where K_u is uniaxial anisotropy constant and $t = t_{RL} + t_{PL}$. We change the relationship between the two terms of the anisotropy field by changing t_{RL}. Thus, we can change the magnetic moments arrange after TMT(2).

Rhombus-shaped microobjects with the angle α = 20 and 40° were fabricated from the films of SVs with t_{RL} = 2.3, 2.5, 3.0, 3.5 and 4 nm. TMT(1) and TMT(2) were performed consistently and then the Wheatstone bridge output voltage was measured in the short diagonal of the rhombus under a magnetic field swept along EA. Figure 13 shows the bar charts for comparison of the Wheatstone bridge U_{out}/U_{in} ratio with the MR_{max} value of SV stripes. For the convenience of the comparison we also plotted the relation between U_{out}/U_{in} and MR_{max} as a function of the reference layer thickness (Figure 14).

Preprints (www.preprints.org) | NOT PEER-REVIEWED | Posted: 5 December 2023 doi:10.20944/preprints202312.0210.v1

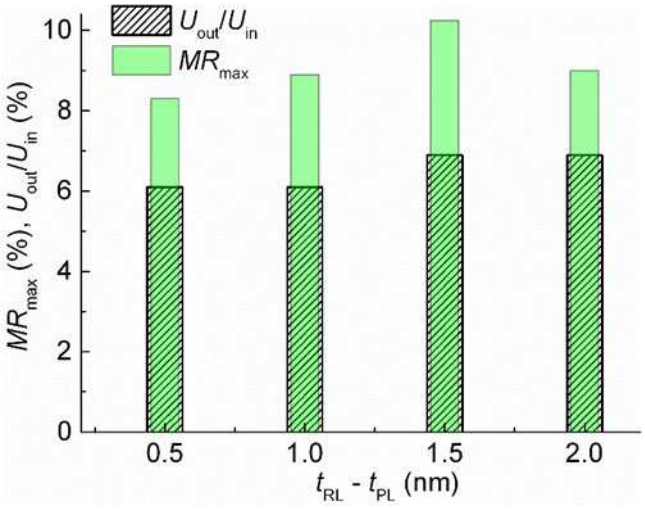

Figure 13. The dependencies of Wheatstone bridge U_{out}/U_{in} ratio and SV stripe MR_{max} value on the thickness of the reference layer for rhombus-shaped microobjects with $\alpha = 40^{o}$.

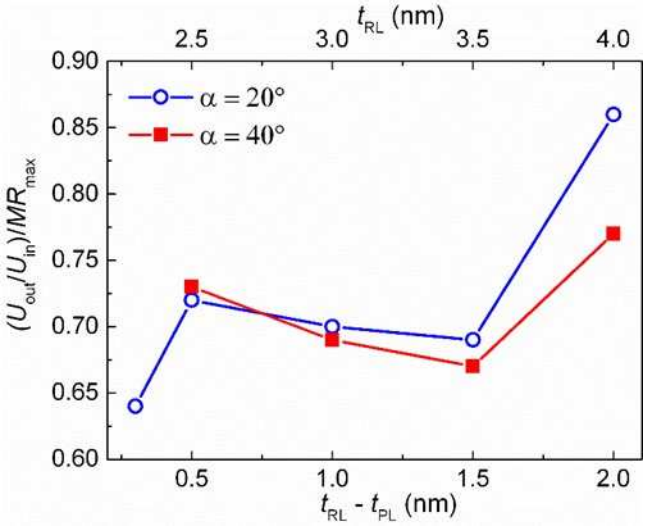

Figure 14. The dependencies of the relation between U_{out}/U_{in} and MR_{max} on the thickness of the reference layer for rhombus-shaped microobjects with $\alpha = 20$ and 40^{o}.

For two sets of the rhombus-shaped microobjects (α = 20 and 40^{o}) the minimal difference between U_{out}/U_{in} and MR_{max} was found for samples with maximum t_{RL} and maximum difference in FM layers thicknesses in SAF. Probably, the effect of shape anisotropy on the alignment of magnetic moments at TMT increases with an increase in the total magnetic moment of antiferromagnetically coupled M_{PL} and M_{RL}.

4. Discussion

The proposed method of implementing the full Wheatstone bridge scheme with SVs as a magnetically sensitive material is quite simple. It does not require separate sputtering of SV elements with an exchange bias opposite in sign and separate TMT of each SV element. Nevertheless, there are a number of requirements for the successful application of this method. To prevent accidental splitting into magnetic domains, the microstructure of the layers should contain a minimum of defects and the interlayer boundaries should be smooth. Opposite in exchange bias SV elements should change magnetoresistance in the same low fields. Therefore, the shift of the low-field hysteresis loop should be close to $H = 0$. To increase the ratio between U_{out}/U_{in} and MR_{max} of each SV

element, it is necessary to increase the difference in the thicknesses of the reference and pinned layer and, accordingly, the total magnetic moment of SAF

5. Conclusions

It is shown that shape anisotropy controls turn of magnetic moments in spin valve microobjects in low magnetic fields.

We found the TMT procedure, which makes it possible to obtain opposite in sign exchange bias fields and a close to collinear arrangement of axes of uniaxial and unidirectional anisotropy in separate elements of Wheatstone bridge circuit. The procedure includes two subsequent TMT in the applied perpendicular to easy axis magnetic field. At the first TMT the field exceed the saturation field and at the second TMT the field is close to $H = 0$. Formation of the opposite exchange bias in non-parallel sides of the rhombus-shaped microobject is caused by the predominance of shape anisotropy in magnetic reversal and during TMT. Output signal of the based on the complete Wheatstone Bridge sensor have the shape of a step. Such characteristic are in demand in switching devices.

Author Contributions. V.U. supervision and project administration , V.P. magnetron sputtering SV films, L.N. design of experiments and analysis of the data, writing of manuscript, X-ray diffractometry, A.G. mi-croobjects fabrication, magnetoresistance measurements, T.C. investigation, thermomagnetic threatment, figure representations and analysis of the data, A.P. magnetic microscopic investiga-tion by atomic force microscopy , T.K. microstructure studies by transmission electron micros-copy, M.M. supervision, review and editing. All authors have read and agreed to the published version of the manuscript.

Funding: This study was performed in terms of state assignment for the Ministry of Science and Higher Education of the Russian Federation (theme Spin, no. 122021000036-3).

Institutional Review Board Statement: Not applicable.

Informed Consent Statement: Not applicable
Conflicts of Interest: The authors declare no conflict of interest.

References

1. Freitas, P.P.; Ferreira, R.; Cardoso, S. Spintronic sensors. *Proceeding of the IEEE* **2016**, *104*, 1894–1918. 10.1109/JPROC.2016.2578303
2. Carvalho, M.; Ribeiro, P.; Romão, V.; S. Cardoso, S. Smart fingertip sensor for food quality control: Fruit maturity assessment with a magnetic device. *Journal of Magnetism and Magnetic Materials* **2021**, *536*, 168116 (1-5). https://doi.org/10.1016/j.jmmm.2021.168116
3. Yan, S.; Cao, Z.; Guo, Z.; Zheng, Z.; Cao, A.; Qi, Y.; Leng, Q.; Zhao, W. Design and Fabrication of Full Wheatstone-Bridge-Based Angular GMR Sensors. *Sensors* 2018, *18*(*6*), 1832 (1-8). https://doi.org/10.3390/s18061832
4. Suharyadi, E.; Alfansuri, T.; Handriani, L. S.; Wibowo, N. A.; Sabarman, H. Detection of Fe3O4/PEG nanoparticles using one and two spin-valve GMR sensing elements in Wheatstone bridge circuit. *Journal of Materials Science: Materials in Electronics* **2021**, *32*, 23958-23967. https://doi.org/10.1007/s10854-021-06859-6
5. Dieny, B.; Speriosu, V.S.; Parkin, S.S.P.; Gurney, B.A.; Wilhout, D.R.; Maui, D. Giant magnetoresistance in soft ferromagnetic multilayers. *Phys. Rev. B.* **1991**, *43*(*1*), 1297–1300.
6. Kools, J.C.S. Exchange-Biased Spin-Valves for Magnetic Storage. *IEEE Trans. on Magn.* **1996**, *32*(*4*), 3165–3184. 10.1109/20.508381
7. Svalov, A.V.; Sorokin, A.N.; Savin, P.A.; García-Arribas, A.; Fernández, A.; Vas'kovskiy, V.O.; Kurlyandskaya, G.V. Co/Cu/Co Pseudo Spin-Valve System Prepared by Magnetron Sputtering with Different Argon Pressure. *Key Engineering Materials* **2015**, *644*, 211–214. https://doi.org/10.4028/www.scientific.net/KEM.644.211
8. Öksüzoglu, R.M.; Sarac, U., Yıldırım M., Çınar H. Characterization of Microstructural and Morphological Properties in As-deposited Ta/NiFe/IrMn/CoFe/Ta Multilayer. *System. J. Mater. Sci. Technol.* **2014**, *30*(*4*), 359–364. https://doi.org/10.1016/j.jmst.2013.10.024
9. Naumova, L.I.; Milyaev, M. A.; Zavornitsin, R. S.; Pavlova, A. Yu.; Maksimova, I. K.; Krinitsina, T. P.; Chernyshova, T. A.; Proglyado, V. V.; Ustinov, V. V. High-Sensitive Sensing Elements Based on Spin Valves with Antiferromagnetic Interlayer. Coupling. *Physics of Metals and Metallography* **2019**, *120* (*7*), 653-659. 10.1134/S0031918X1907007X

10. Meguro, K.; Hoshiya, H.; Watanabe, K.; Hamakawa, Y.; Fuyama, M. Spin-Valve Films Using Synthetic Ferrimagnets for Pinned Layer. *IEEE Trans. on Magn*. **1999**, *35* (*5*), 2925-2927. 10.1109/20.801029
11. Huai, Y.; Zhang, J.; Anderson, G.W.; Rana, P.; Funada, S.; Hung, C.Y.; Zhao, M.; Tran. S. Spin-valve heads with synthetic antiferromagnet CoFe/Ru/CoFe/IrMn. *Journal of Applied Physics* **1999**, *85*(*8*), 5528-5530. https://doi.org/10.1063/1.369883
12. Milyaev, M.; Naumova, L.; Chernyshova, T.; Proglyado, V.; Kamensky, I.; Ustinov, V. Spin-flop in Synthetic Antiferromagnet and Anhysteretic Magnetic Reversal in FeMn-Based Spin Valves. *IEEE Trans. on Magn.* **2016**, *52*, 2301104-. 10.1109/TMAG.2016.2593424
13. Milyaev, M.A.; L.I. Naumova, L.I.; Zavornitsyn, R.S.; Maksimova, I.K.; A.Yu. Pavlova, A.Yu.; Proglyado, V.V.; Ustinov, V.V. Use of a Spin-Flop State for the Creation of Spin-Valve Elements for a Full Wheatstone Bridge. *Physics of Metals and Metallography* **2020**, *121* (*8*), 721-728. 0.1134/S0031918X20080050
14. Ferreira, R.; Paz, E.; Freitas, P.; Ribeiro, J.; Germano, J.; Sousa, L. 2-Axis Magnetometers Based on Full Wheatstone Bridges Incorporating. Magnetic Tunnel Junctions Connected in Series. *IEEE Trans. on Magn.* **2012**, *48* (*11*), 4107. 10.1109/TMAG.2012.2202381
15. Borole, U.P.; Khan, J.; Barshilia, H.C.; Chowdhury,P. Design, fabrication, and characterization of giant magnetoresistance (GMR) based open-loop current sensor with U-shaped current carrying conductor. *Sensors Actuators A* **2021**, *332*, 112103 (1-10). https://doi.org/10.1016/j.sna.2021.113103
16. Fukuzawa H., Iwasaki H., Koi K., Sahashi M. Soft magnetic characteristics of an ultrathin CoFeNi free layer in spin-valve films *J. Magnetism and Magnetic Mater* **2006**, *298*, 65–71. https://doi.org/10.1016/j.jmmm.2005.03.010
17. Sugita, Y.; Kawawake, Y.; Satomi, M.; Sakakima H. Thermal stability of PtMn based synthetic spin valves using thin oxide layer. *J. Appl,. Phys.* **2001**, *89*(*11*), 6919–6921. https://doi.org/10.1063/1.1359221
18. Bannikova, N. S.; Milyaev, M. A.; Naumova, L. I.; Patrakov, E. I.; Proglyado, V. V.; Kamenskii, I. Yu.; Ryabukhina, M. V.; Ustinov, V. V. Giant Magnetoresistance and Hysteresis Phenomena in CoFe/Cu Superlattices with Highly Perfect Crystallographic Texture. *Physics of Metals and Metallography* **2018**, *119* (*11*), 1073-1078. 10.1134/S0031918X18110029
19. Bannikova, N. S.; Milyaev, M. A.; Naumova, L. I.; Krinitsina, T. P.; Patrakov, E. I.; Proglyado, V. V.; Chernyshova, T. A.; Ustinov, V. V. NiFeCo/Cu superlattices with high magnetoresistive sensitivity and weak hysteresis. *Physics of the Solid State* **2016**, *58* (*10*), 2011-2017. 10.1134/S1063783416100061
20. Berkowitz, A.E.; Takano, K. Exchange anisotropy - a review. *J. Magn. Magn. Mat.* **1999**, *200*, 552-570. https://doi.org/10.1016/S0304-8853(99)00453-9
21. Tong, H.C.; Qian, C.; Miloslavsky, L.; Funada, S.; Shi, X.; Liu, F.; Dey, S. The spin flop of synthetic antiferromagnetic films *J. Appl. Phys.* **2000**, *87*, 5055-5067. https://doi.org/10.1063/1.373246
22. Beach, R.S.; McCord, J.; Webb, P.; Mauri, D. Orthogonal pinning of two ferromagnetic layers in a synthetic spin valve *Appl. Phys. Lett.* **2002**, *80*, 4576–4578. https://doi.org/10.1063/1.1485106
23. Reig, C.; Cubells-Beltran, M.-D.; Munoz, D.R.; Magnetic Field Sensors Based on Giant Magnetoresistance (GMR) Technology: Applications in Electrical Current Sensing. *Sensors* **2009**, *9*, 7919–7942. https://doi.org/10.3390/s91007919
24. Osborn, J.A. Demagnetizing Factors of the General Ellipsoid. *Phys. Rev.* **1945,** *67* (*11–12*), 351 - 357.